MESON–MESON AND MESON–NUCLEON SYSTEMS*

J. SPETH, H. HOLTMANN, G. JANSSEN AND C. SCHÜTZ

Institut für Kernphysik, Forschungszentrum Jülich GmbH
52425 Jülich, Germany

(Received January 5, 1995)

Effective meson Lagrangians are the appropriate theoretical tool for the non–perturbative regime of QCD. We introduce the concept of effective Lagrangians and apply it to meson–meson and meson–nucleon scattering. It is shown that with these information one is able to calculate also form factors of mesons and baryons. The same model can be applied to the calculation of quark distributions in baryons and mesons. The recently observed $\bar{u} - \bar{d}$ asymmetry is explained within the meson–cloud model in a natural way.

PACS numbers: 14.40.-n, 11.15.Tk

1. Introduction

The understanding of the structure of hadrons and the interaction between them is the most important unsolved problem in medium-energy physics. Nowadays, quantum chromodynamics (QCD) is considered to be the underlying theory of the strong interaction, with quarks and gluons as fundamental degrees of freedom. In the perturbative regime, that means at short distances which are probed with high momentum transfer, QCD results obtained within perturbation theory agree quantitatively with the experimental data. However, QCD does not yet provide much help in producing a description of the structure of the strongly interacting particles at large distances, *i.e.* lower momentum transfer, since solving the QCD equations for a many-body system in the non-perturbative regime is at the present stage far beyond our abilities. Therefore it is still important to construct models and constrain them by experimental information. For us it seems important that such models should be able to describe aspects of the

* Presented at the XXIX Zakopane School of Physics, Zakopane, Poland, September 5–14, 1994.

non-perturbative as well as the perturbative regime. In the first one mesons and baryons have definitely retained their importance as efficient, collective degrees of freedom for a wide range of nuclear phenomena. Meson-exchange models for the strong interaction and the vector-dominance for the electromagnetic form-factors of the proton and pion are well-known examples. However there is increasing evidence that also the sea-quark distribution of hadrons can be described within the same meson-exchange models.

Our modern picture of hadrons is that of a core of valence quarks surrounded by a sea of $q\bar{q}$ pairs and gluons. For low energy processes (up to a few GeV) it seems that much of the detailed dynamics of the quarks can be neglected and the cloud can be approximated by the correlated, color-neutral $q\bar{q}$ states that we know as mesons. This is the basis of the success of the meson-exchange models. It is obvious that such a description must eventually break down. At some energy scale, the quark and gluonic degrees of freedom must become important. The question is, at what energy this does occur. Clearly, this is connected with the size of the quark confinement region. Since the radii of hadrons are given by the confining region as well as the meson cloud, the range of applicability of the meson-cloud model may be much larger than thought from naive estimates based on physical sizes.

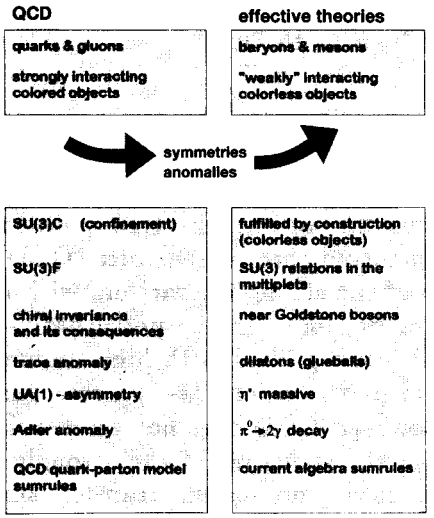

Fig. 1. A possible scenario for the construction of effective theories using the symmetries of the QCD Lagrangian.

What we need in the non-perturbative regime is an effective theory with baryons and mesons as the relevant degrees of freedom. To construct the appropriate Lagrangian we use the symmetries of the QCD-Lagrangian as

guideline. We show in Fig. 1 how this can be done. The starting point of our calculations is the non-linear σ-model with vector-mesons introduced as gauge-bosons [1, 2]. In Fig. 2 the effective Lagrangian in the SU(2) meson sector is shown.

$$L_{\text{eff}} = \tfrac{1}{2}\partial_\mu \vec{\pi}\partial^\mu \vec{\pi} - \tfrac{1}{2}m_\pi^2 \vec{\pi}^{\,2} + g\vec{V}_\mu(\vec{\pi} \times \partial^\mu \vec{\pi}) - \tfrac{1}{4}\vec{F}_{\mu\nu}\vec{F}^{\mu\nu} + \tfrac{1}{2}m_\rho^2 \vec{V}_\mu \vec{V}^\mu + \cdots$$

$$F^a_{\mu\nu} = \partial_\mu V^a_\nu - \partial_\nu V^a_\mu + g\varepsilon^{abc} V^b_\mu V^c_\nu$$

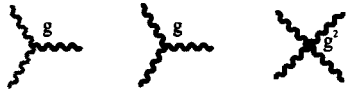

$$L_{\text{QCD}} = \bar{\Psi}(i\not{D} - M)\Psi - \tfrac{1}{4}F^a_{\mu\nu}F^{\mu\nu}_a$$

$$D_\mu = (\partial_\mu - igA_\mu); \quad A_\mu \equiv \frac{\lambda^a}{2}A^a_\mu$$

$$F^a_{\mu\nu} = \partial_\mu A^a_\nu - \partial_\nu A^a_\mu + gf^{abc}A^b_\mu A^c_\nu$$

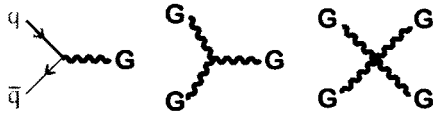

Fig. 2. Comparison of an effective meson theory (non-linear σ-model with vector–mesons) with QCD. The lighter lines in the upper part indicate pseudoscalar mesons and the darker ones vector mesons. In the lower part the lighter and darker lines indicate quarks and gluons, respectively.

In the following we shall discuss three topics:

(i) Meson–meson scattering, where we concentrate on the scalar-isoscalar resonances seen in $\pi\pi$ scattering and on the A_1 meson which shows up in $\pi\rho$ scattering. We also demonstrate that these quantities are connected with the electromagnetic form factor of the pion and the strong pion–nucleon form factor.

(ii) Pion–nucleon scattering: Here we analyse the πN phase shifts. As a new feature, we replace the fictitious σ meson and the zero-width ρ meson used in most of the previous attempts by the correlated two-pion exchange, discussed in the first section. We obtain excellent agreement with the data with a reduced number of parameters.

(iii) Sea-quark distribution: For an understanding of the transition region from baryon–meson to quark–gluon it is crucial that our model is able

to describe some new and important features of the sea quarks. We shall show that the violation of the Gottfried sum rule and the corresponding x-dependence of $\bar{u}(x) - \bar{d}(x)$ finds its natural explanation in the meson-exchange model.

2. Meson–meson scattering

2.1. $\pi\pi$ scattering

The interaction between two pions is the most fundamental meson-meson interaction and of paramount importance for many parts of medium-energy physics. The determination of isoscalar and isotensor $\pi\pi$ scattering lengths provides an important test of chiral symmetry predictions and the low-energy behavior of the $\pi\pi$ scattering amplitude ($E < 1$ GeV) is, *e.g.*, relevant for nucleon-nucleon physics. For higher energies, open questions concerning meson spectroscopy are closely related to the $\pi\pi$ interaction, *e.g.* the nature of the $f_0(975)$ or the search for the members of the scalar nonet. Finally, a knowledge of the full off-shell $\pi\pi$ scattering amplitude is desirable for several applications; in particular, we will discuss the electromagnetic pion form factor.

To obtain a realistic model for $\pi\pi$ scattering our group has applied the concepts of the meson-exchange framework to calculate the coupled-channel potentials for $\pi\pi \to \pi\pi$, $\pi\pi \to K\bar{K}$ and $K\bar{K} \to K\bar{K}$ [3, 4]. The potential contains t-channel vector-meson exchanges (ρ, K^*, ω, ϕ) as well as s-channel diagrams (ρ, $f_0(1400)$, $f_2(1270)$) and is iterated in a relativistic scattering equation of Lippmann–Schwinger type,

$$T = V + VG_0T\,. \tag{1}$$

All coupling constants are determined either from the decay widths of the corresponding particles (*e.g.* $g_{\rho\pi\pi}$) or from SU(3) symmetry relations (*e.g.* $g_{\rho KK} = {}^1\!/_2\, g_{\rho\pi\pi}$). In addition, standard formfactors have been included at each three-meson vertex to take into account the extended structure of the involved hadrons; the corresponding cutoff masses are the free parameters of our model.

Fig. 3 shows the result of our fit to the available data sets for several partial waves (data are referenced in [3]). It demonstrates that we obtain quite good overall agreement with the experimental situation. In particular, we are able to describe the structure appearing around 1.0 GeV in the isoscalar $\pi\pi$ S-wave which is assigned to the f_0 meson. In our model this resonance-like behavior is generated dynamically by the strong attraction arising from ρ, ω and ϕ exchange in the $K\bar{K}$ channel and we therefore do *not* need a genuine scalar resonance with mass around 1.0 GeV (this is

demonstrated for δ_{00} by the dashed line in Fig. 3 where we have excluded any s-channel pole diagram). On the other hand, however, it is definitely necessary to include a heavy scalar particle, namely the $f_0(1400)$ with mass around 1.4 GeV, to describe the experimental data beyond 1.0 GeV (full line in Fig. 3). For smaller energies ($E_{\mathrm{cms}} \leq 1$ GeV) the $\pi\pi$ S-wave is characterized by a very large phase shift dominantly generated by ρ exchange (dotted line in Fig. 3).

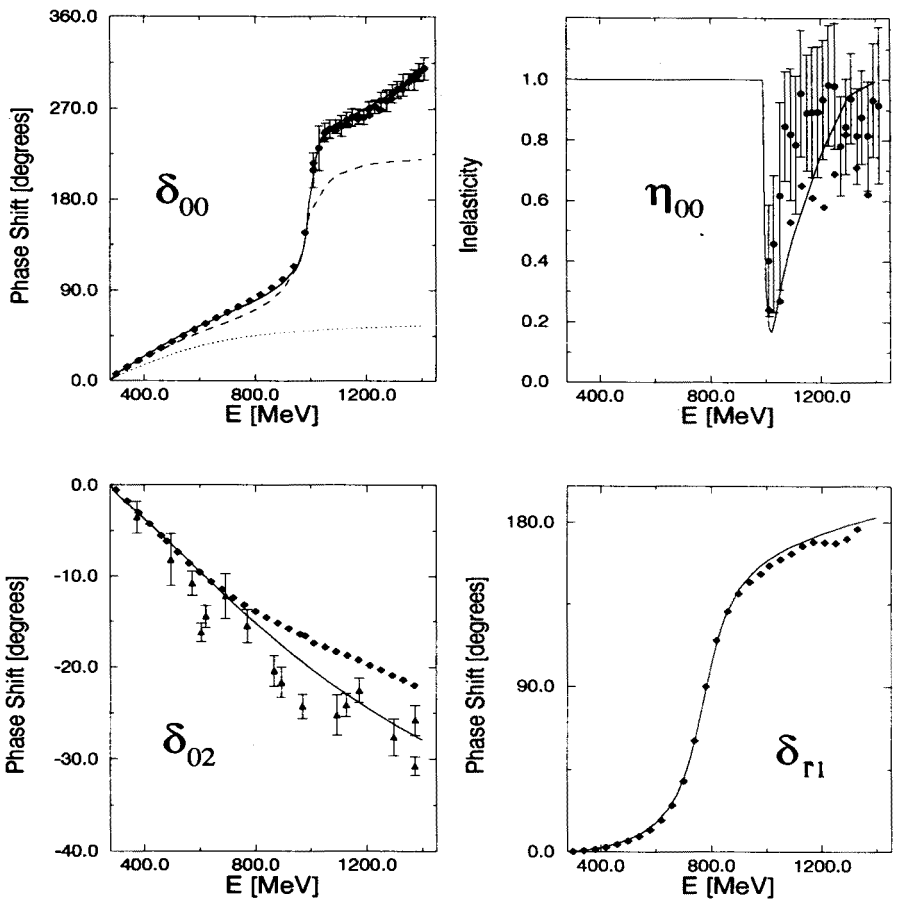

Fig. 3. Results of our $\pi\pi$ scattering model in comparison with experimental data. The solid line shows the result of our full model. For the dashed line in δ_{00} we have excluded the $f_0(1400)$ pole diagram whereas the dotted line includes only the $\pi\pi \rightarrow \pi\pi$ potential.

TABLE I

$\pi\pi$ scattering lengths

	$a_0^0\ [m_\pi^{-1}]$	$a_2^0\ [m_\pi^{-1}]$
Full Jülich model	0.307	−0.037
Chiral pert. theory	0.200	−0.042
Burkhardt and Lowe [5]	0.197 ± 0.010	-0.032 ± 0.004
Modified Jülich model, Rapp	0.210	−0.028

Table I shows our result for the isoscalar and isovector $\pi\pi$ scattering lengths compared to other sources showing reasonable agreement. It was already pointed out that the $\pi\pi$ low-energy parameters are closely related to chiral symmetry; several soft-pion theorems can be derived using the assumption of chiral invariance but most of them are related to crossing symmetry which in our model is only satisfied at the level of Born diagrams. The minimal constraint imposed by chiral symmetry, however, is the requirement of scattering lengths linearly depending on the pion mass as m_π goes to zero. Again, the iteration of the Born-level potential in a scattering equation makes it difficult to fulfil this requirement but with a properly chosen off-shell behavior the right m_π dependence of a_0^0 and a_2^0 can be obtained [Fig. 4, Table I (Modified Jülich model, Rapp)].

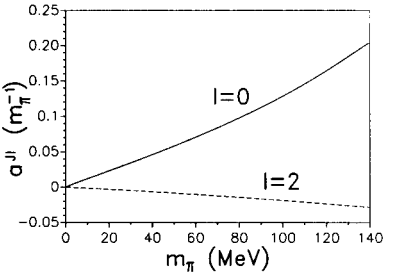

Fig. 4. The $\pi\pi$ scattering lengths as m_π goes to zero in the modified Jülich model (Rapp).

Having obtained a model which is able to satisfy experimental and theoretical constraints quite well we turn our attention to the electromagnetic pion form factor. Fig. 5 shows the basic ingredients of our extended vector-dominance model (VDM). (Though the figure contains both electromagnetic and scalar pion form factors, we will restrict ourselves to the former one). Compared to the simple VDM our calculation is based on a more microscopic picture including a bare ρ meson (ρ^0) which is dressed by the full $\pi\pi$ interaction resulting in an energy-dependent selfenergy and width. Fig. 6 shows the result of our calculation in the time-like and space-like region

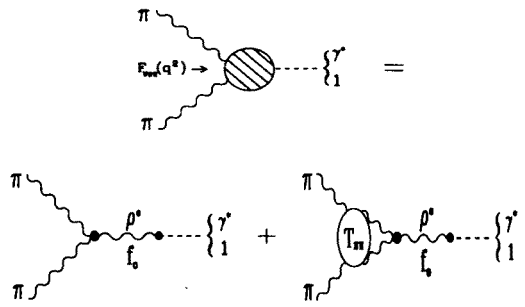

Fig. 5. The extended VDM model for the electromagnetic pion formfactor.

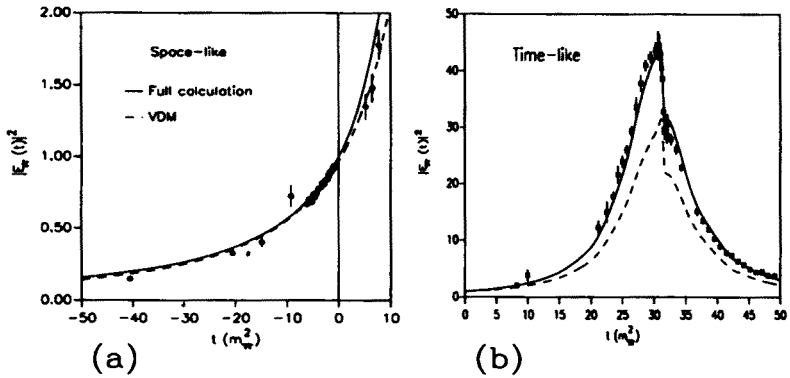

Fig. 6. Results for the electromagnetic pion form factor in the time-like and space-like region. The solid line shows the result of our full microscopic model, the dashed curve is obtained from the vector-dominance model (VDM).

demonstrating a considerable improvement in the description of the data compared to the simple VDM result.

2.2. $\pi\rho$ scattering

In the preceding section the concepts of the meson-exchange framework have successfully been applied to the most fundamental meson-meson process, namely $\pi\pi$ scattering. Here, we will extend the corresponding formalism to the $\pi\rho$ system and demonstrate its relevance for several processes of medium-energy physics. In particular, we will show that our model for $\pi\rho$ scattering can remove apparent discrepancies in the analysis of the A_1 meson. Furthermore, it will be applied to calculate the πNN form factor leading to an appreciable softening of the corresponding cutoff mass.

As for the $\pi\pi$ system the $\pi\rho$ potential contains several t-channel exchange contributions (π, ω, ρ) as well as s-channel pole diagrams (A_1, ω).

Difficulties arise due to the fact that the ρ meson is quite unstable, *i.e.* in principle one must solve the underlying three-pion problem. It has been shown [6], however, that all main results remain unchanged if the ρ is treated as a stable particle and a simple two-body scattering equation [Eq. (1)] is used to iterate the $\pi\rho$ potential.

We first consider the $L_{JT} = S_{11}$ partial wave, *i.e.* the A_1-channel. Here, ρ-exchange provides the dominant exchange contribution; however, a genuine A_1-pole term is definitely needed in order to obtain agreement (by adjusting open parameters) with the mass spectrum seen in hadronic processes like $\pi^- p \to \pi^+\pi^-\pi^0 n$ [7] and shown in Fig. 7.

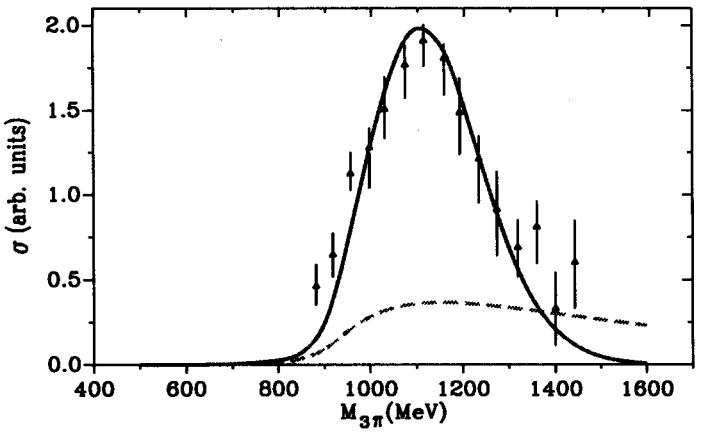

Fig. 7. The result for the A_1 mass spectrum. The solid line shows our full model; for the dashed curve only the non-pole background is included.

From these data, the resonance mass appears to be at 1.13 GeV [7] with a width of about 0.3 GeV. However, this conclusion is spoiled by the presence of the sizable non-pole amplitude T_{np} (dashed in Fig. 7), which shifts the maximum of the mass spectrum away from the true resonance position. Indeed, if we determine in our theoretical model the location of the pole of the scattering amplitude in the complex plane, the mass and width actually come out to be at $m_{A_1} = 1.26$ GeV and $\Gamma_{A_1} = 0.43$ GeV. This result is in nice agreement with an analysis [8] of the decay of the τ-meson which gives the most reliable values for the A_1 parameters.

What is important is that there is obviously a large non-pole contribution to the $\pi\rho$ interaction, whose size can be correctly constrained by the empirical data in the A_1-channel. This non-pole contribution now acts in all other channels, *e.g.* in the pionic ($L_{JT} = P_{01}$) channel, with a definite strength distribution, which is characteristic of the underlying model.

Having obtained a realistic description of $\pi\rho$ scattering our model is applied to the calculation of the πNN form factor. Since the $\pi\rho$ scattering amplitude is not constructed in an explicitly crossing-symmetric way we first have to evaluate the form factor in the t-channel ($N\bar{N} \to \pi\rho \to \pi$). The total $N\bar{N}\pi$ vertex function is generated by the diagrams shown in Fig. 8 where the $N\bar{N} \to \pi\rho$ transition interaction $V_{\pi\rho,N\bar{N}}$ is obtained from a meson-exchange model with nucleon (N) and delta-isobar (Δ) exchange. Since we are interested in the form factor in the s-channel of the NN system a once-subtracted dispersion integral is then applied to obtain the form factor for $t < 0$.

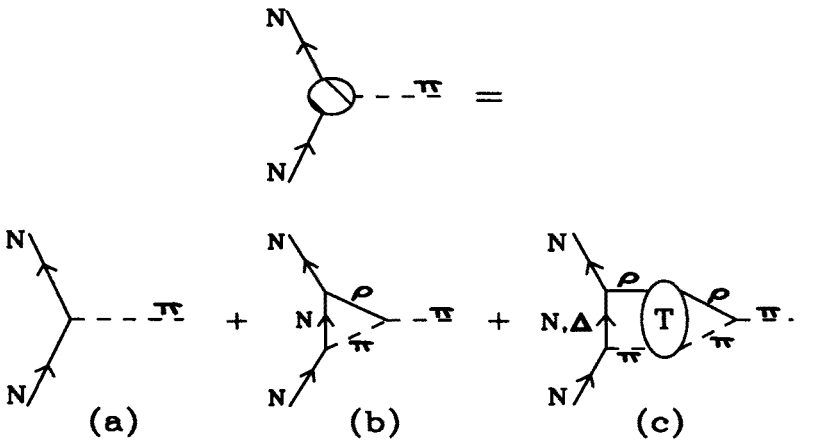

Fig. 8. Diagrams contributing to the πNN form factor.

Results are shown in Fig. 9. Obviously, the inclusion of the $\pi\rho$ interaction (diagram 8(c)) leads to a remarkable shift, yielding a much softer form factor, corresponding to a cutoff mass $\Lambda_{\pi NN}$ of about 1 GeV [9]. This result is in agreement with information from several other sources requiring a soft πNN vertex. The final value for $\Lambda_{\pi NN}$ depends somewhat on vertex parameters in diagram 8 (b), (c), but our main result, the relative shift in $\Lambda_{\pi NN}$ as a manifestation of a strong $\pi\rho$ interaction, turns out to be rather stable.

It should be mentioned at this point that a soft πNN form factor causes serious problems for meson-exchange NN potentials since it suppresses the tensor-force and destroys the reproduction of the deuteron properties. It has been shown [10], however, that the $\pi\rho$ interaction is not only important for the πNN form factor but provides an additional contribution to the NN potential, namely correlated $\pi\rho$ exchange. This contribution generates additional tensor-force and counterbalances the effect of the soft πNN form factor thus restoring the description of the NN data.

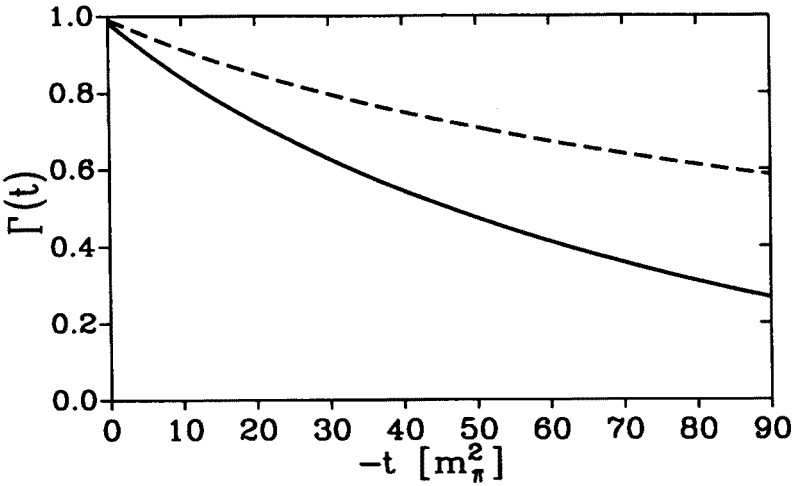

Fig. 9. The result for the πNN form factor in the space-like region. The solid line shows our full model; for the dashed curve no $\pi\rho$ rescattering is included. The solid line corresponds to a monopole parametrization with $\Lambda_{\pi NN}=1$ GeV.

3. Pion–nucleon interaction

The interaction between a pion and a nucleon plays an outstanding role in low- and medium-energy physics. First, it is of topical interest in itself, being a prominent example of a strong hadronic interaction. Second, it is an important ingredient in many other reactions, *e.g.* pion photo-production, pion production in nucleon–nucleon collisions or scattering of a pion on a nucleus.

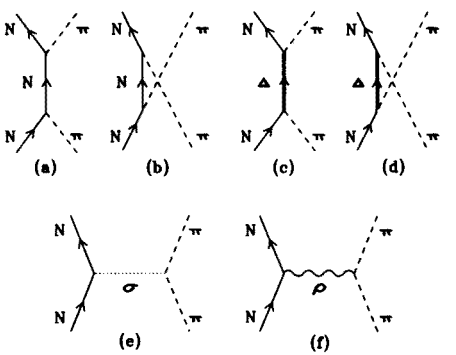

Fig. 10. Diagrams included in the πN potential.

Recently, several papers have been published, which present a meson-exchange model for πN scattering [11–14]. All these models include the

direct and crossed nucleon as well as Δ-isobar pole terms, see Fig. 10 (a)–(d). Furthermore they all contain some kind of σ- and ρ-exchange contributions. Here the situation is very confusing because different coupling schemes and parameters are used in the various approaches.

In a more microscopic treatment, σ- as well as ρ-exchange should be viewed as correlated two-pion exchange processes in the scalar–isoscalar resp. vector–isovector channel (*cf.* Fig. 10 (e), (f)). As is well-known for the NN system, this provides constraints on the size of σ and ρ exchange. Therefore in a recent work [15] we have developed such a model for correlated two-pion exchange in the pion–nucleon interaction. Starting from the investigation of the reaction $N\bar{N} \to \pi\pi$ in the pseudophysical region (below threshold of the $N\bar{N}$ system) these processes are calculated using dispersion integral techniques.

In a second step this model of correlated 2π-exchange is then supplemented by conventional (direct and exchange) pole diagrams involving the nucleon and Δ isobar, *cf.* Fig. 10 (a)–(d), (which are treated as bare particles in case of the direct terms) and the interaction is then unitarized by means of the relativistic Schrödinger equation

$$T(Z) = V + V\frac{1}{Z - H_0}T(Z) \tag{2}$$

which dresses the direct pole terms by shifting their masses and providing a width (in the case of the Δ) generated by the dynamics of the model.

3.1. πN phase shifts

After solving the scattering equation the partial wave πN phase shifts are calculated in the standard way. Results are shown in Fig. 11 in comparison to the empirical phase shifts obtained from an analysis of Koch and Pietarinen [17]. We obtain a good agreement in all partial waves. For details about the parameters used in this calculation we refer the reader to Ref. [15].

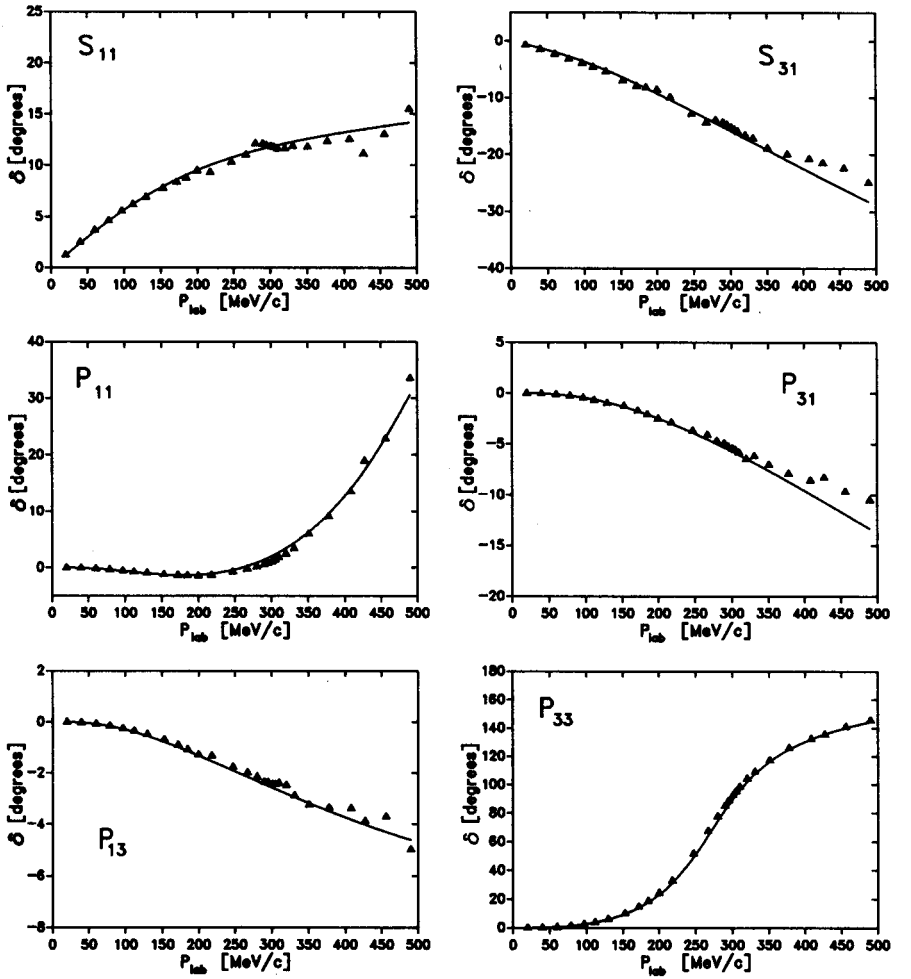

Fig. 11. πN scattering phase shifts in S and P waves, as functions of the pion laboratory momentum. The empirical information is taken from Ref. [17].

3.2. Low energy parameters

For our πN interaction model, the resulting scattering lengths and volumes, defined as

$$a_L = \lim_{q \to 0} \frac{\sin 2\delta_L}{2q^{2L+1}} \tag{3}$$

are in good agreement with the empirical information, as shown in Table II.

TABLE II

The scattering lengths and volumes. Units are $m_\pi^{-(2L+1)}$

	model	Koch and Pietarinen [17]
S_{11}	0.169	0.173 ± 0.003
S_{31}	−0.085	-0.101 ± 0.004
P_{11}	−0.080	-0.081 ± 0.002
P_{31}	−0.043	-0.045 ± 0.002
P_{13}	−0.031	-0.030 ± 0.002
P_{33}	0.210	0.214 ± 0.002

3.3. πN Σ term

According to the Cheng–Dashen theorem [18], the isospin-even forward scattering amplitude at the Cheng–Dashen point is given by

$$T^{(+)}(\nu = 0, \nu_B = 0, q^2 = m_\pi^2, q'^2 = m_\pi^2) = \frac{\Sigma}{f_\pi^2}, \tag{4}$$

where Σ denotes the πN Σ term and f_π the weak pion decay constant. Using this relation, an extrapolation of our dynamical model below threshold of the πN system enables us to calculate the πN Σ term. This provides an important test whether a model, which agrees with the empirical situation in the physical region, also satisfies chiral symmetry constraints. The result of our model is 65.5 MeV which is in good agreement with the experimental value of $\Sigma = 60 \pm 10$ MeV [19]. (Note that here $\Sigma(2m_\pi^2)$ has been evaluated. In an earlier work on the scalar form factor of the nucleon [20], we have found within the same framework a 15 MeV contribution to the Σ term arising from the difference $\Sigma(2m_\pi^2) - \Sigma(0)$.)

3.4. P_{11}-wave πN scattering and the Roper resonance

One of the most interesting partial waves in πN scattering is the P_{11} partial wave. It is a challenge for models of πN interaction to describe quantitatively the repulsion at low energies followed by the attraction leading to the Roper resonance at higher energies. Within the model presented here, the rise of the P_{11} phase shift in the elastic region of the interaction can be reproduced without any contribution from a genuine N^* particle. In Fig. 12 (a) we have plotted the on-shell potential (*i.e.*the Born term) in this partial wave split into its pole part, which is generated by the direct nucleon pole, and the non-pole part. This non-pole part of the interaction is dominated by correlated 2π exchange in the ρ channel. Whereas the pole part of the

potential is repulsive the non-pole part is attractive over the whole energy range investigated here. This attraction is so strong that the iteration of the non-pole part of the potential even leads to resonant behavior in this partial wave at relatively low energies ($\simeq$ 1.3 GeV, *cf.* . Fig. 7 (b)). If this attraction is counterbalanced by the direct nucleon pole contribution, the data (in the elastic region) can be described quantitatively.

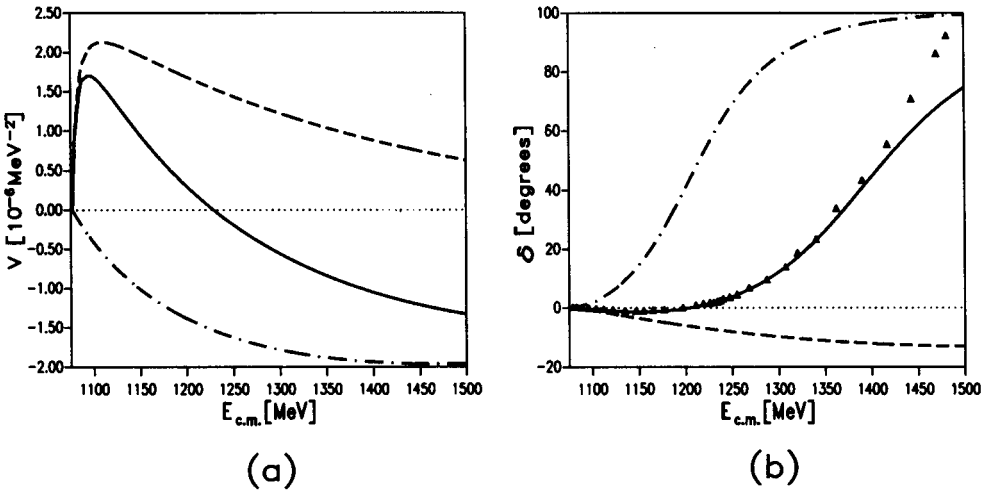

Fig. 12. (a) — On-shell potentials in the P_{11} partial wave as functions of the c.m.s. energy. The dashed line arises from the direct nucleon pole; the dash-dotted line belongs to the non-pole part of the potential; the solid line gives the total potential. (b) — Resulting phase shifts after iteration of the corresponding contributions to the potential. Empirical data points are taken from Ref. [16].

For energies above 1.3 GeV, the pion–nucleon interaction becomes inelastic. According to the 'Review of Particle Properties' [21], the branching ratio of the Roper resonance into the $\pi\pi N$ channel is 30–40%. Here the dominant contributions are the $\pi\Delta$ channel (20–30%) and the σN channel (5–15%), where σ denotes an isoscalar $\pi\pi$ S-wave state.

As a first step, we have investigated the coupled channel system $\pi N - \sigma N$, where in our model the additional contributions shown in Fig. 13 are taken into account. The (effective) σNN coupling is taken from Ref. [22]. Self-energy contributions of the σ are implemented in our calculation. As one can see from Fig. 14, inclusion of these additional processes leads to a resonant behavior in the P_{11} partial wave. However, not surprisingly, the model accounts only for part of the inelasticity. Here the additional effect of the reaction channel $\pi\Delta$ remains to be investigated.

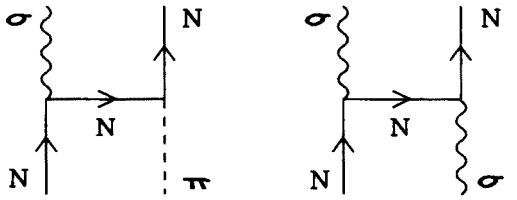

Fig. 13. Additional contributions to our interaction model.

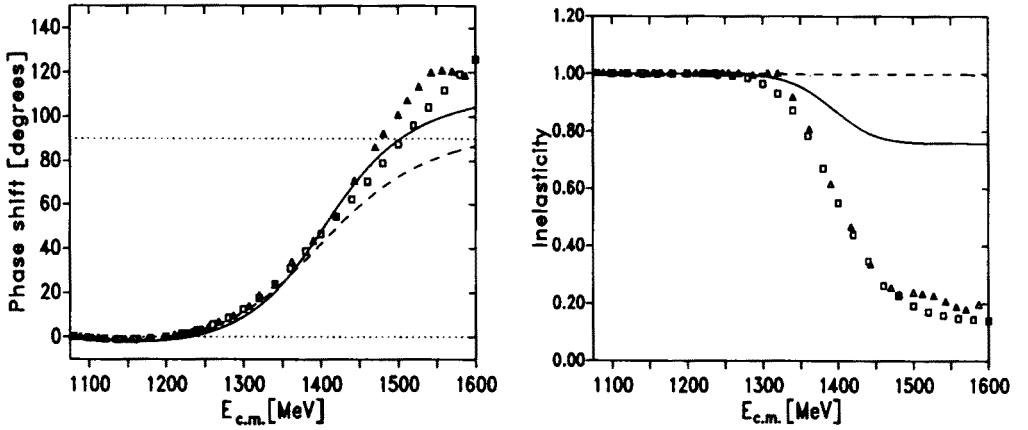

Fig. 14. The $\pi N - \sigma N$ coupled channel calculation (solid lines) compared to the one-channel calculation (dashed lines). Squares (triangles) denote the empirical information from Ref. [23] (Ref. [16]).

4. Meson-exchange and deep-inelastic scattering

In deep-inelastic scattering the structure of the proton can be probed. This is done by scattering high-energy electrons on a proton (Fig. 15). The corresponding differential cross section is given by:

$$\frac{d^2\sigma}{dx\,dy} = \frac{8\pi\alpha^2}{mEx^2y^2}\left\{xy^2F_1(x) + \left(1 - y - \frac{m}{2E}xy\right)F_2(x)\right\}, \qquad (5)$$

where $x = Q^2/2m\nu$ and $y = \nu/E$. $-Q^2$ is the squared four-momentum of the exchanged virtual photon, ν its energy. E is the energy of the ingoing electron. The process can be interpreted that the virtual photon does not react with the whole proton but with one of its constituents (partons) which has a longitudinal momentum fraction x with respect to the proton momentum. By measuring the differential cross section over a large range of x, y

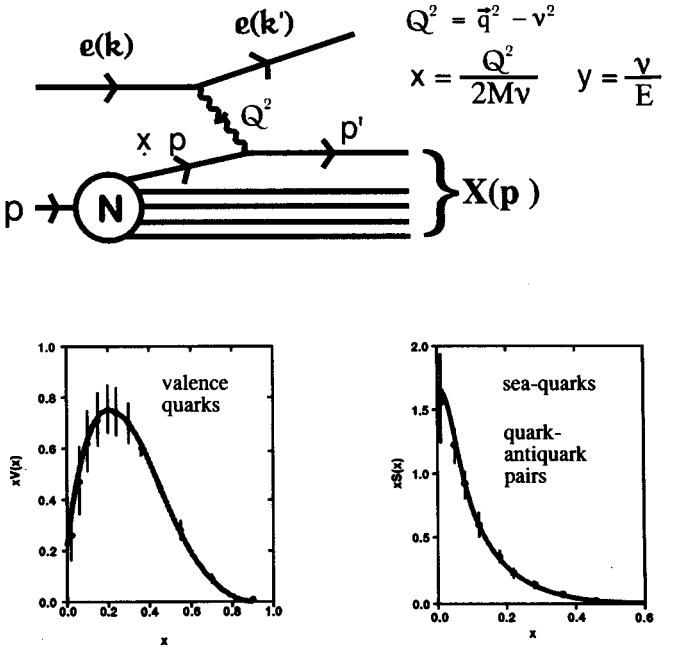

Fig. 15. Schematic figure of deep-inelastic electron-scattering off a nucleon (note that a 'realistic' nucleon consists of more than three quarks). We also show the valence- and sea-quark distribution of a proton.

the structure functions $F_1(x)$ and $F_2(x)$ can be extracted. In the parton model (for details see *e.g.* [24]) these structure functions can be expressed using the quark distribution functions $u(x)$, $d(x)$, $s(x)$, $\bar{u}(x)$, $\bar{d}(x)$ and $\bar{s}(x)$ (there are of course also distribution functions for the other 3 quark flavors, but because of their smallness they can be neglected safely in the following discussion):

$$F_1(x) = \tfrac{1}{2}\left(\tfrac{4}{9}(u(x)+\bar{u}(x)) + \tfrac{1}{9}(d(x)+\bar{d}(x)) + \tfrac{1}{9}(s(x)+\bar{s}(x))\right), \quad (6)$$

$$F_2(x) = x\left(\tfrac{4}{9}(u(x)+\bar{u}(x)) + \tfrac{1}{9}(d(x)+\bar{d}(x)) + \tfrac{1}{9}(s(x)+\bar{s}(x))\right). \quad (7)$$

A standard result of perturbative QCD is that the nucleon sea is flavor symmetric ($\bar{d}(x) = \bar{u}(x)$), because anti-quarks can only be produced from gluons which do not carry any flavor. This leads directly to the Gottfried Sum Rule

$$S_G = \int_0^1 \left[F_2^p(x) - F_2^n(x)\right] \frac{dx}{x} = \tfrac{1}{3} + \tfrac{2}{3}\int_0^1 \left[\bar{u}_p(x) - \bar{d}_p(x)\right] dx = \tfrac{1}{3}. \quad (8)$$

The NMC measurement of the Gottfried Sum Rule [25], $S_G^{exp} = 0.24 \pm 0.16$, provides experimental evidence that the nucleon sea is not flavor symmetric.

A complete description of the experimental data requires $\int_0^1 (\bar{d}_p(x) - \bar{u}_p(x))dx = 0.135 \pm 0.024$.

This shows that some essential feature of the quark distributions can only be described using non-perturbative physics. The idea we want to present here, is that the quarks inside a nucleon are condensed into colorless hadrons. This leads to the assumption that the proton has a component consisting of, *e.g.*, a bare proton plus a π^0 or a bare neutron plus a π^+ and indeed, this gives a natural explanation for the excess of $\bar{d}$ quarks. In our approach we include all the mesons and baryons required in the description of the low-energy nucleon-nucleon and hyperon-nucleon scattering. More formally the proton state can be written as a sum of various meson-baryon Fock states

$$|p\rangle = \frac{1}{Z}[|p\rangle_{\mathbf{bare}} + n_{\pi N}|\pi N\rangle + n_{\rho N}|\rho N\rangle + n_{\pi\Delta}|\pi\Delta\rangle + n_{\rho\Delta}|\rho\Delta\rangle + \cdots], \quad (9)$$

where $Z = 1 + \sum_{MB} n_{MB}$ is a wave function renormalization constant and n_{MB}/Z gives the probability that the proton is in a state consisting of a meson M and a baryon B. The exact expressions for n_{MB} can be found in [26, 27]. The presence of higher meson–baryon Fock-states in the proton has the consequence that the virtual photon, in addition to scattering off the proton itself, can also scatter off a meson or recoil baryon (Fig. 16). The evaluation of these diagrams leads to the convolution model (or Meson-Cloud Model) [26–28].

Sullivan-process:

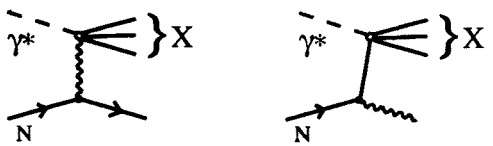

meson off-shell nucleon off-shell

Fig. 16. Contribution to deep-inelastic scattering from meson-baryon Fock-states: (a) scattering off a meson, (b) scattering off a recoil baryon.

The main ingredients of our model are the vertex coupling constants and the vertex form factors which account for the extended nature of the hadrons. The coupling constants are assumed to be related via SU(3) symmetry and were taken from the Bonn-NN potential model [29]. The only free parameters are the cut-offs of the vertex form factors. They can be fixed by using the high-energy $p(p,n)X$, $p(h,\Delta^{++})X$, $p(p,\Lambda)X$ production data assuming a one-meson exchange model (Fig. 17, for details see [30]).

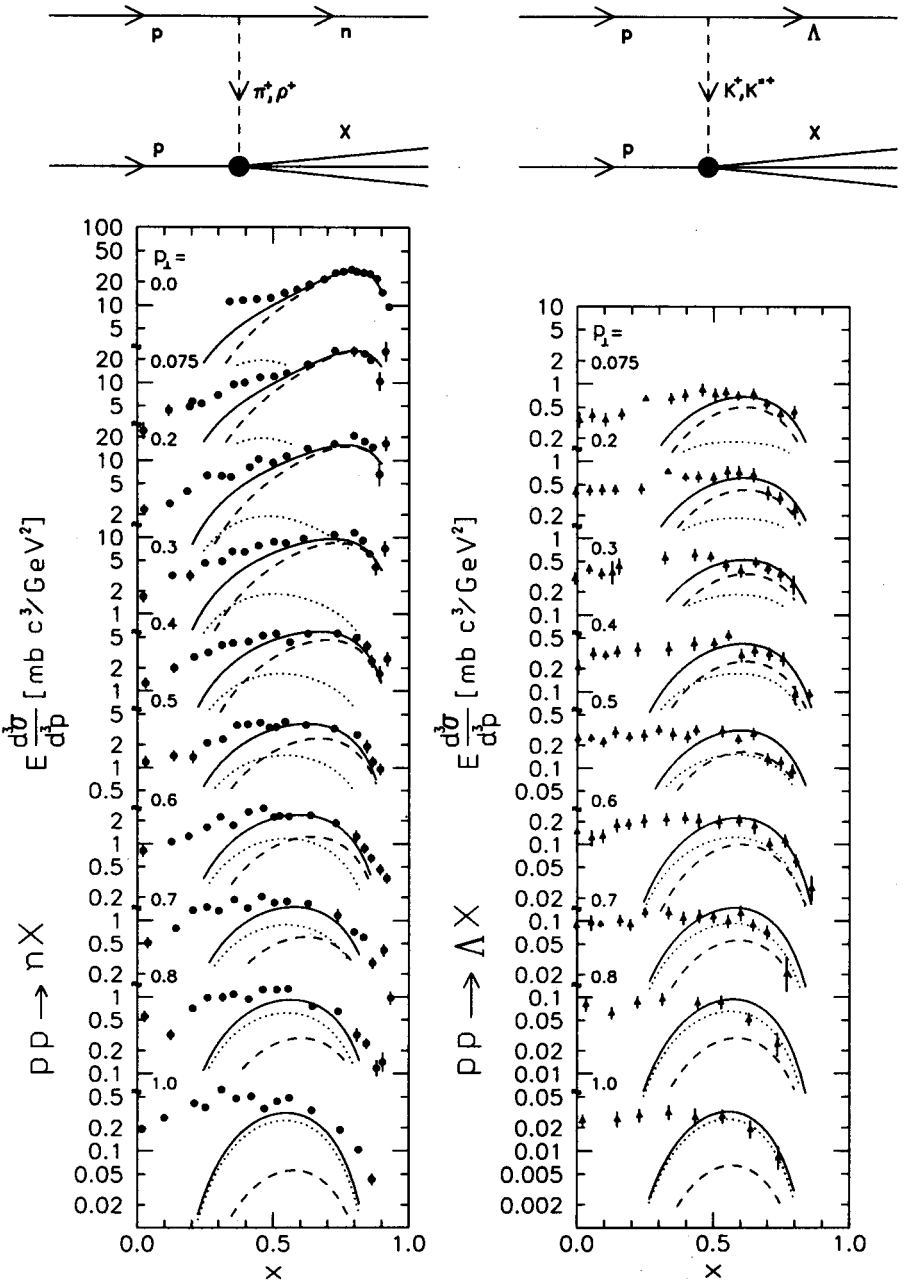

Fig. 17. Fit of the $N\pi N$ ($N\rho N$, $NK\Lambda$, $NK^*\Lambda$) form factors using n, Λ production in high-energy pp scattering. x is the longitudinal momentum fraction of the outgoing neutron (Λ), $p_\perp$ its transversal momentum. The contribution from the $\pi(K)$ exchange are denoted by a dashed line, the $\rho(K^*)$ exchange by a dotted line (sum: solid line).

The data prefer a cut-off of $\Lambda = 1.08$ GeV for processes involving virtual octet baryons and $\Lambda = 0.98$ GeV for processes with virtual decuplet baryons using an exponential form factor

$$\exp\Big(\frac{1}{2\Lambda}(m_N^2 - M_{MB}^2)\Big)\,, \tag{10}$$

with m_N being the nucleon mass and M_{MB}^2 being the squared invariant mass (total four-momentum squared) of the Fock state under consideration. The value obtained for the Gottfried Sum Rule is $S_G = 0.224$ and it lies within the experimental errors of the NMC experiment.

Further evidence for the violation of the $\bar{u}$-$\bar{d}$ symmetry is given by a recent Drell–Yan result. The NA51 collaboration has found [31]

$$\frac{\bar{u}(x)}{\bar{d}(x)} = 0.51 \pm 0.04 \pm 0.05 \qquad \text{at } x = 0.18\,. \tag{11}$$

This ratio can also be calculated within our model. For this calculation we need as additional input the bare quark distributions (*i.e.*the quark distributions of the proton without contributions from meson-baryon Fock states). They can be obtained by fitting them, using the convolution formalism for the higher meson-baryon Fock states, to the experimental data [32]. After these bare quark distributions have been fixed, the $\bar{u}(x)/\bar{d}(x)$ ratio can be calculated (Fig. 18). Also for this observable an excellent agreement with the experiment can be noticed.

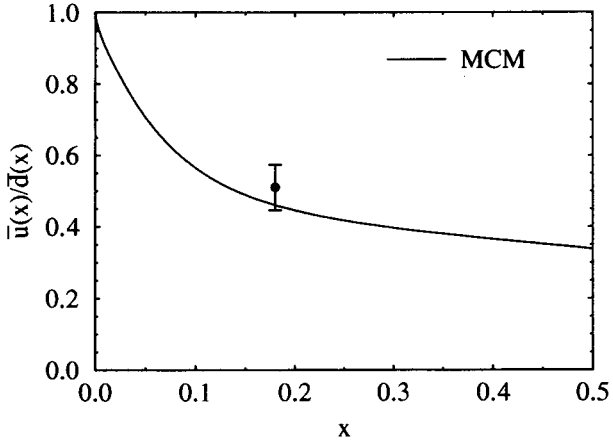

Fig. 18. The $\bar{u}(x)/\bar{d}(x)$ ratio calculated in our model. The data point is from the NA51 collaboration.

Together with the result for the Gottfried Sum Rule there is now ample evidence that a large part of the sea in the nucleon is induced non-perturbatively by mesons.

The Fock-state expansion, Eq. (9), not only applies to deep-inelastic scattering, but also to low-energy properties of the nucleon. Recently, we have analyzed the consequences induced by our model for the electromagnetic form factors [33, 34] of the proton and the neutron. To evaluate the effects of the our model we have fitted the bare form factors, assuming a dipole form for the Sachs form factors G_p^E, G_p^M and G_n^M (G_n^E was assumed to vanish), to the experimental data. The most interesting result we found was that the simple assumption $G^E_{n,\mathrm{bare}} = 0$ together with the πN Fock state is sufficient to describe the experimental measured G_n^E data (Fig. 19). This calculation includes up to now only the πN Fock state, it will be extended shortly.

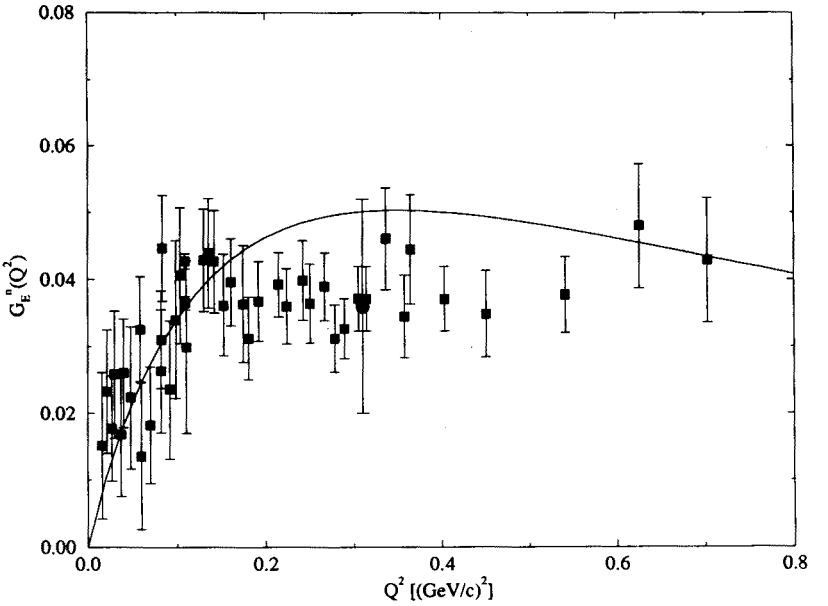

Fig. 19. The electric neutron form factor G_n^E in our model (solid line). The data was taken from [35] (squares) and [36] (circle).

5. Conclusions

We have investigated a few selected phenomena in both the "low"-energy scattering regime and deep-inelastic scattering. We find that the concept of the meson cloud, although very old, is still a useful and powerful tool. It gives a quite natural explanation for many phenomena related to hadron structure, which have been under investigation in the last few years.

The model of the $\pi\pi - K\bar{K}$ system we have reviewed is driven by s- and t-channel meson exchanges with the vertices obtained from an SU(3) symmetric Lagrangian. Only the well-established mesons $(\rho, \omega, \phi, K^*(892))$ are used in the t-channel driving terms. The $f_0(975)$ then emerges as a $K\bar{K}$ bound state. The phase shifts beyond 1 GeV make it necessary to include a state corresponding to the $f_0(1400)$. We have also presented results for the pion electromagnetic form factor in the space- and time-like region which agrees well with the data. The same model is applied to $\pi\rho$ scattering and the strong πNN form factor. Here it turned out that this form factor is relatively soft because the pion couples preferentially through the $\pi\rho$-coupling to the nucleon. If we use the $\pi\pi$ scattering results for πN scattering we obtain theoretical πN phase shifts which agree well with the data.

Within our model we get in a very natural way SU(2) flavor symmetry breaking in the nuclear sea. The difference between $\bar{u}$ and $\bar{d}$ distributions leads automatically to a violation of the Gottfried sum rule and makes a prediction for the x-dependence of this effect. Finally we showed that the same model with the same parameters which explains the Gottfried sum rule also reproduces the electric form factor of the neutron.

We thank Karl Holinde, Mikkel Johnson, Antony Szczurek, and Tony Thomas for discussions. This work was supported in part by the Humboldt senior fellow program, the German Academic Exchange Service (HSP II), and the Science & Technology Cooperation Germany/Canada (KAN-BSC13).

REFERENCES

[1] S. Weinberg, *Phys. Rev.* **166**, 1568 (1968).
[2] M. Bando, T. Kugo, K. Yamawaki, *Nucl. Phys.* **B259**, 493 (1985).
[3] D. Lohse, J.W. Durso, K. Holinde, J. Speth, *Nucl. Phys.* **A516**, 513 (1990).
[4] B.C. Pearce, K. Holinde, J. Speth, R. Tegen, Few Body Systems **Suppl. 6**, 50 (1992).
[5] H Burkhard, J. Lowe, *Phys. Rev. Lett.* **67**, 2622 (1991).
[6] G. Janssen, K. Holinde, J. Speth, *Phys. Rev.* **C49**, 2763 (1994).
[7] J.A. Dankowych *et al.*, *Phys. Rev. Lett.* **38**, 580 (1981).
[8] M.G. Bowler, *Phys. Lett.* **209B**, 99 (1988).
[9] G. Janssen, J.W. Durso, K. Holinde, B.C. Pearce, J. Speth, *Phys. Rev. Lett.* **71**, 1978 (1993).
[10] G. Janssen, K. Holinde, J. Speth, *Phys. Rev. Lett.* **73**, 1332 (1994).
[11] B.C. Pearce B.K. Jennings, *Nucl. Phys.* **A528**, 655 (1991).
[12] C. Lee, S.N. Yang, T.-S. H. Lee, *J. Phys.* **G17**, L131 (1991).
[13] F. Gross Y. Surya, *Phys. Rev.* **C47**, 703 (1993).

[14] P.F.A. Goudsmit, H.J. Leisi, E. Matsinos, *Phys. Lett.* **B299**, 6 (1993); P.F.A. Goudsmit, H.J. Leisi, E. Matsinos, B.L. Birbrair, A.B. Gridnev, *Nucl. Phys.* **A575**, 673 (1994).
[15] C. Schütz, J.W. Durso, K. Holinde, J. Speth, *Phys. Rev.* **C49**, 2671 (1994).
[16] G. Höhler, *Pion–Nucleon Scattering*, Landolt–Börnstein Vol.I/9b2, ed. H. Schopper, Springer 1983.
[17] R. Koch, E. Pietarinen, *Nucl. Phys.* **A336**, 331 (1980).
[18] T.P. Cheng, R. Dashen, *Phys. Rev. Lett.* **26**, 594 (1971).
[19] J. Gasser, H. Leutwyler, M.E. Sainio, *Phys. Lett.* **B253**, 252 (1991).
[20] B.C. Pearce, K. Holinde, J. Speth, *Nucl. Phys.* **A541**, 663 (1992).
[21] Review of Particle Properties, *Phys. Rev.* **D45**, Part 2 (June 1992).
[22] J.W. Durso, A.D. Jackson, B.J. Verwest, *Nucl. Phys.* **A345**, 471 (1980).
[23] R.A. Arndt, VPI analysis FA93, private communication.
[24] F. Close, *An Introduction to Quarks and Partons* , Academic Press, London 1979.
[25] P. Amaudruz *et al.*, *Phys. Rev. Lett.* **66**, 2712 (1991).
[26] V.R. Zoller, *Z. Phys.* **C53**, 443 (1992).
[27] H. Holtmann, A. Szczurek, J. Speth, *Jülich preprint KFA-IKP(TH)-1993-33,* submitted to *Phys. Rev.* **D**.
[28] A. Szczurek J. Speth, *Nucl. Phys.* **A555**, 249 (1993).
[29] R. Machleidt, K. Holinde, Ch. Elster, *Phys. Rep.* **149**, 1 (1987).
[30] H. Holtmann, A. Szczurek, J. Speth, *Jülich preprint KFA-IKP(TH)-25* (1994) submitted to *Phys. Rev.* **D**.
[31] A. Baldit *et al.*, *Phys. Lett.* **B332**, 244 (1994).
[32] H. Holtmann, A. Szczurek, J. Speth, paper in preparation .
[33] N.N. Nikolaev, A. Szczurek, J. Speth, V.R. Zoller, *Z. Phys.* **A349**, 59 (1994).
[34] H. Holtmann, A. Szczurek, J. Speth, *Jülich preprint KFA-IKP(TH)-1994-33,* submitted to *Z. Phys.* **A**.
[35] S. Platchkov *et al.*, *Nucl. Phys.* **A510**, 740 (1990).
[36] M. Meyerhoff *et al.*, *Phys. Lett.* **B327**, 201 (1994).